Canonical proper time quantum gravitation

James Lindesay

Computational Physics Laboratory, Department of Physics, Howard University, Washington, DC 20059

E-mail: jlindesay@howard.edu

Abstract. At the root of the tensions involved in modeling the quantum dynamics of gravitating systems are the subtleties of quantum locality. Quantum mechanics describes physical phenomena using a theory of non-local phase relationships (non-local in the sense that quantum states maintain a space-like coherence that is acausal). However, the principle of equivalence in general relativity asserts that freely falling frames are locally inertial frames of reference. Thus, gravitating systems are often described using constituents that are freely falling, undergoing geodesic motion defining well localized trajectories. The canonical proper time formulation of relativistic dynamics is particularly useful for describing such inertial constituents using the coordinates of non-inertial observers. The physics of the simplest of gravitating inertial quantum systems, consistent with presented experimental evidence, will be examined. Subsequently, descriptions of both weakly and strongly gravitating quantum systems will be developed using canonical proper gravitation.

1. Introduction

Quantum mechanics remains an enigmatic formulation when examined through intuitions framed in classical mechanics. Some of the fundamentals of quantum mechanics are itemized as follows:

- Measurements cannot be objectified in quantum physics. Certain physical parameters (like position and momentum) cannot be simultaneously measured in a single measurement.
- Quantum formulations of physical systems inherently incorporate unknown and unknowable quantities (as demonstrated in EPR entanglements[1], and Bell's hidden variable analysis[2]).
- What *can* be known about a quantum coherent system is contained in its quantum state vector $|\Psi\rangle$, state components Ψ_m, or wave function $\Psi(x,t)$, and probabilities $\Psi^*_m\Psi_m$ or $\Psi^*(x,t)\Psi(x,t)dx$.
- A given system is not the wavefunction itself, since wavefunctions can only be used to describe outcome likelihoods consistent with physical conservation laws. The system will be measured to be in one state or another, not spread amongst a set of states. This is even true of classical distributions of unmeasured states. However, for classical distributions the constituent states of an ensemble can in principle be known on some level.

As an illustration of the difference between a classically coherent system and a quantum coherent system, consider a wave-front propagating through space. For a classical ocean wave breaking upon a beach, each floating plankton and grain of sand on the beach is a detector of the classically coherent wave. However, for a quantum wave breaking upon detectors, there

is no intermediate detection, and only one detector will measure the particle, resulting in a "collapse of the wavefunction" describing its propagation. Subsequence to that detection, the description of the quantum system provided by the prior wavefunction becomes obsolete. Any measurement of a quantum system fixes the immediate past of that system to be consistent with that particular measurement, but leaves any future measurements uncertain while the system remains coherent.

The double slit experiment provides a good demonstration of inherent quantum behaviors. In the double slit experiment illustrated in Figures 1, particles are incident from the left upon a solid wall that has only two slits through which any particle can pass without being absorbed. Classical particles either hit the barrier or hit the screen on the right, clustering just behind the

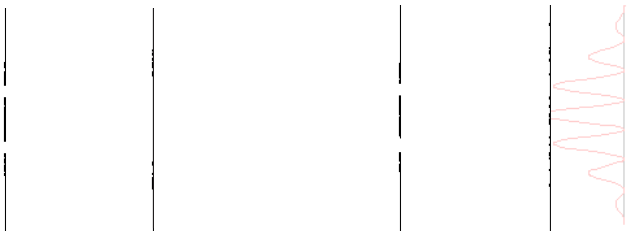

Figure 1. *Illustration of the result of 100 particles incident from the left upon a barrier with two horizontal slits for classical particles (left) vs quantum particles (right).*

slits. However, quantum particles are singly detected on the screen on the right in a distribution that is widely spread over the screen in a manner characterized by a wave that coherently passes through both slits. Notice that if the quantum particles are continuously observed, they behave like the classical particles. Furthermore, if any quantum particle is detected going through either slit, the particle is later detected as if it were just a classical particle (or perhaps diffracted wave) going only through that slit. Particles that are not detected going through either slit maintain space-like quantum coherence throughout the propagation and self-interfere going through both slits. Any measurement that localizes the propagation of the particle through one slit or the other breaks its coherence. The phase relationships in this experiment are determined purely by the classical geometry, and remain unchanged irregardless of any motions of the observer.

There are general constraints upon measurements of quantum systems. If one makes many measurements upon a set of identically prepared quantum coherent systems, the average of those measurements satisfy the uncertainty principle $\Delta x\, \Delta p \geq \frac{\hbar}{2}$, where ΔQ is the root mean squared deviation of measurements of quantity Q from its average value. This principle follows from the triangle identity for the magnitudes of two state vectors and their resultant, and the non-commutivity of the momentum and position operators[3]. This non-commutivity prevents *any* single measurement of both the momentum and position of a quantum state.

The incorporation of the non-local behaviors of quantum systems into gravitation is not trivial. If the gravitational interaction itself is to be quantized, the non-linear effects become particularly difficult to understand, especially for strongly gravitating systems. Also, experimental evidence presented in the next section demonstrates that gravitational quanta *cannot* be the mechanism by which space-time localization occurs during the gravitation of quantum coherent systems. In other words, space-time coordinates cannot "bubble up" during the quasi-stationary gravitation of coherent systems in a manner that localizes regions of those systems. The coordinates themselves cannot be entangled with the systems.

Classical gravitation is unique amongst interactions in that vastly differing objects with identical geometric initial conditions will follow identical trajectories, allowing the geometrization of gravitational dynamics. Locally, the motions of objects are essentially the same as those of inertial objects as viewed by accelerating observers, allowing descriptions of

the dynamics in terms of various coordinate representations of those motions. The *principle of equivalence* effectively equates the inertial mass of an object with the mass determining the strength of gravitational coupling. This characteristic of gravity allows classical motions of arbitrary local objects in terms of unique *geodesics* independent of gravitational couplings. Covariance then allows one to use *any* convenient coordinates to describe those motions.

What follows will explore the consequences of the principle of equivalence on the gravitation, co-gravitation, and self-gravitation of quantum coherent systems. Section 2 summarizes some of the experiments involving quantum gravity, illustrates inertial systems as viewed by accelerating observers, and develops canonical proper gravitation. Section 3 explores some properties of a non-singular black hole, in particular demonstrating that quantum non-locality can in principle prevent gravitational collapse to a singularity. Finally, section 4 will briefly discuss the modeling of gravitating quantum fields.

2. Gravitation and Quantum Coherence

2.1. Experiments in Quantum Gravity

During the 1970's, experiments[4] were performed on quantum coherent neutrons undergoing self-interference in the Earth's gravitational field. Those experiments involved a form of double slit interference illustrated in Figure 2. In the experiment, singly traversing neutrons are counted

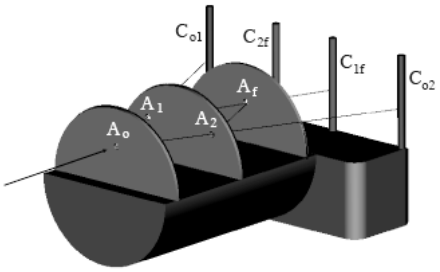

Figure 2. *Diagram of apparatus used to demonstrate quantum coherence of gravitating neutrons. Neutrons incident upon aperture A_o self-interfere through apertures A_1 and A_2, and are detected via counters C_{1f} and C_{2f} for which no classical trajectory for the neutrons exists.*

at the two counters C_{1f} and C_{2f} for which no classical trajectory exist for the incident neutrons. The apparatus is then rotated about the axis of incidence of the neutrons, changing the relative gravitational potential (and therefore the relative phase) between A_1 and A_2. The formulation of the interference pattern in the expected difference in counts between the counters requires use of both Newton's constant G_N and Planck's constant $\hbar$ in same formula, which was verified by the experiment. One could therefore conclude that gravitating quantum systems maintain spatial coherence. This means that gravitational interactions cannot break quantum coherence in order to establish spatial and temporal relationships, despite common interpretations that gravity *is* geometry. The establishment of the space-time geometry that localizes the propagation of each neutron through the slits cannot also localize the gravitating neutron at either slit. The experiment verifies the principle of equivalence for a quantum system, which will here be stated as follows: *The coherence state of an inertial system is not affected by the motions of the observer.* The result from the Earth-based laboratory should be indistinguishable from the result on an accelerating spaceship and apparatus with incident inertial neutrons.

Other experimental observations have demonstrated the maintenance of quantum coherence during gravitation:

- Interference in ticks of quantum atomic clocks superposed across differing gravitational potentials due to Compton frequencies (temporal coherence)[5].
- Wannier-Stark ladders (interference between fermions on rungs of an optical ladder[6]), which can be used as precise gravimeters[7].
- CMB photons maintain coherence for 14 billion years over a change in cosmological scale of 1100 (very dynamic!), while sometimes undergoing gravitational lensings.
- Red-shift / time dilation effects are important even for everyday behaviors of Global Positioning Satellites (GPS), resulting in a shift of +46ms/day from gravity and -7ms/day from motions (the GPS system requires 50 nanoseconds/day accuracy)[8].
- Precession of superfluid vortex arrays in Earth's gravitational field.

One can interpret these observations as demonstrating that the establishment of geometric relationships in a quantum coherent gravitating system does not break quantum coherence.

2.2. Uniform Proper Acceleration

Examine the differential Lorentz transformation from the (momentary) rest frame of a system with constant proper acceleration $(c\tau, z_P)$ to an inertial Minkowski frame (ct, z) expressed in terms of the rapidity ζ:

$$\begin{aligned} dct &= \cosh\zeta\, dc\tau + \sinh\zeta\, dz_P, \\ dz &= \sinh\zeta\, dc\tau + \cosh\zeta\, dz_P. \end{aligned} \tag{2.1}$$

For an observer at rest in the proper frame of reference, (2.1) implies that

$$v_P = \frac{dz_P}{dc\tau} = 0 \quad \Rightarrow \quad \frac{dct}{dc\tau} = \cosh\zeta\,,\ \frac{dz}{dct} = \tanh\zeta. \tag{2.2}$$

Since the direction of acceleration remains unchanged, the rapidities characterizing the Lorentz velocity transformations add, implying that

$$\frac{v'}{c} = \tanh(\zeta + \zeta') \quad \Rightarrow \quad \frac{\delta v_P}{c} = \tanh(\delta\zeta) = \delta\zeta. \tag{2.3}$$

This directly relates the proper acceleration a to the rapidity ζ:

$$\frac{dv_P}{d\tau} \equiv a,\ \frac{d\zeta}{d\tau} = \frac{a}{c} \ \rightarrow\ \zeta = \frac{a\tau}{c}. \tag{2.4}$$

Therefore, the solution for the trajectory undergoing uniformly accelerating motion using special relativity is given by

$$\begin{aligned} z(\tau) &= z_P + \tfrac{c^2}{a}\left(\cosh\tfrac{a\tau}{c} - 1\right), \\ t(\tau) &= \tfrac{c}{a}\sinh\tfrac{a\tau}{c}, \\ \tfrac{v(\tau)}{c} &= \tanh\tfrac{a\tau}{c} \end{aligned} \tag{2.5}$$

where z_P is the proper coordinate of the accelerating system, a is the proper acceleration of that system, and τ is the proper time coordinate for that system. The system is seen to be undergoing hyperbolic motion.

2.2.1. Clocks and redshifts

A particularly useful coordinate system can be developed using a spatially dependent form for the local proper acceleration[9]:

$$a = \frac{c^2}{z_P}. \tag{2.6}$$

Using this identification for the proper accelerations in (2.5), all of the trajectories with proper locations z_P approach a single outgoing light-like asymptote passing through the origin, which is a (shared) horizon with proper coordinate $z_P = 0$. The coordinates for an inertial observer (ct, z) corresponding to accelerating coordinates $(c\tau, z_P)$ satisfy

$$ct = z_P \sinh \frac{c\tau}{z_P}\,, \quad z = z_P \cosh \frac{c\tau}{z_P}\,. \tag{2.7}$$

Direct coordinate transformation properties can immediately be developed between the inertial observer and the accelerating observers within the shared causal patch of space-time.

A depiction of two such accelerating trajectories (2.7) is shown in Figure 3. In the figure, all

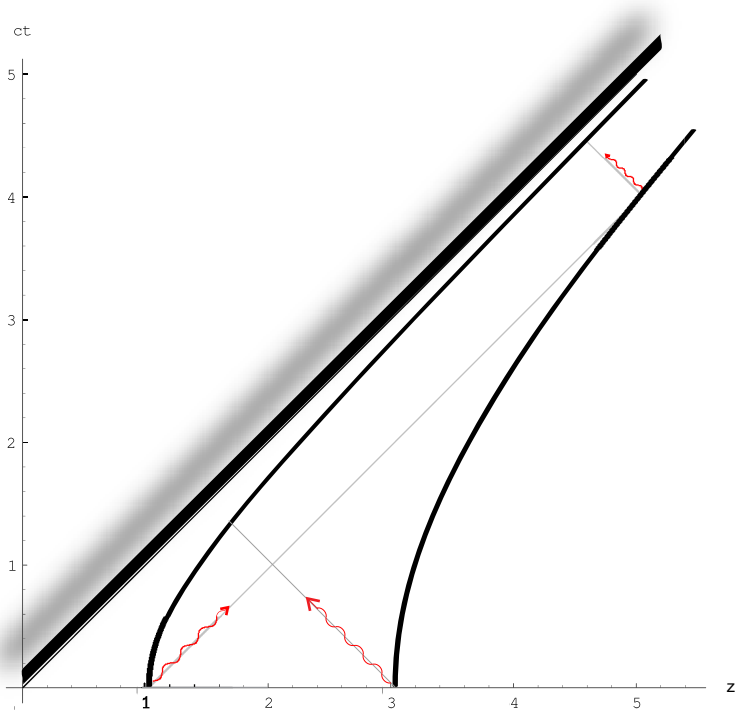

Figure 3. *The traversal of light rays as detected by uniformly accelerating observers, and their usefulness in constructing a standard clock.*

observers with accelerating coordinates are momentarily at rest relative to the inertial observers at $t = 0 = \tau$, with momentarily corresponding proper locations $z = z_P$. This surface represents a surface of synchronicity for the accelerating clocks with the inertial clocks. The trajectories of $z_P = 1$ and $z_P = 3$ are depicted by bold hyperbolas, and the shared horizon of the accelerating observers $z_P = 0$ is depicted as the outgoing light-like bold line through the origin of the Minkowski coordinates.

One can compare the temporal dilations for the different accelerating observers by examining the detection of two light beams emitted simultaneously by two observers towards each other at

$\tau = 0 = t$, as demonstrated in Figure 4. In the first (bottom) frame, the clocks at two separate proper coordinates are synchronized at $\tau = 0$ as the rod is momentarily at rest with respect to the Minkowski frame, and the photons are emitted at each location towards the other. In the second frame, the ingoing photon has traversed along a greater proportion of the proper intervals than has the outgoing photon. By the third frame, the ingoing photon has reached the innermost observer at the proper time demonstrated on the left clock, as the outgoing photon continues towards the outermost observer. The outgoing photon finally reaches the outermost observer in the fifth frame at the proper time indicated. The innermost observer detects a blue-shifted photon, and has a slower moving clock, relative to the outermost observer.

A standard clock can be constructed by the observers in Figure 3 using a photon emitter/detector facing outward at the innermost observer, and a mirror facing inward held by the outermost observer. One tick of such a clock is depicted by the emission of an outgoing photon and the detection of it's reflection. Such a standard clock will tick in the uniformly accelerating system with uniform ticks $\Delta\tau$.

2.3. An Inertial Wavefront Described Using Accelerating Coordinates

Next, the propagation of an inertial neutron as it passes through a uniformly accelerating double slit will be examined. The neutron will be assumed to move with a uniform momentum in the x-direction, while the double slit barrier and detector will be assumed to uniformly accelerate in the z-direction. A wavefront of the neutron is depicted from various perspectives in the illustrations in Figure 5. In the leftmost set of sequential frames, the wavefronts, slits, and detector are displayed on the Minkowski ct-z plane, with the x-direction of propagation suppressed, in sequential snapshots as the proper time of each of the various observers progresses. The incident particle wavefront is displayed in the lower frames as a gray plane progressing upward with fixed z coordinate, becoming cylindrical surfaces after traversing the slits in the upper frames. The asymptotes of the accelerating observer are drawn as the gray light cone with apex at the origin, the double slit barriers are accelerating black solid lines, and the detector is an accelerating black rectangle.

The middle frames in Figure 5 demonstrate the perspective of an inertial observer as the wavefront approaches the uniformly accelerating barrier in the lower frames, becoming interfering wavefronts in the upper frames prior to encountering the accelerating detector. This represents the perspective from which the dynamics can be calculated most directly. The wavefront is a vertical plane prior to the barrier, and interfering cylindrical surfaces subsequent to the barrier. The frames on the right are from the perspective of the accelerating barrier and detector. From this perspective, the approaching wavefront is no longer a vertical planar surface, and the interfering surfaces droop due to the acceleration prior to detection.

2.4. Canonical Proper Gravitation

The canonical proper time formulation for relativistic systems[10, 11] can be quite useful in providing insights into the dynamics of inertial systems using the coordinates of accelerating observers. The canonical proper time generator K is defined to generate translations in the proper time τ of the observed system using the observers' coordinates via

$$[K, z^j(\tau)] = i\hbar \frac{d}{d\tau} z^j(\tau) \quad , \quad [K, p_j(\tau)] = i\hbar \frac{d}{d\tau} p_j(\tau) \, . \tag{2.8}$$

These commutation relations are consistent with the proper time "Hamilton" equations given by

$$\frac{\partial K}{\partial p_j} = \frac{dz^j}{d\tau} \quad , \quad \frac{\partial K}{\partial z^j} = -\frac{dp_j}{d\tau} \, . \tag{2.9}$$

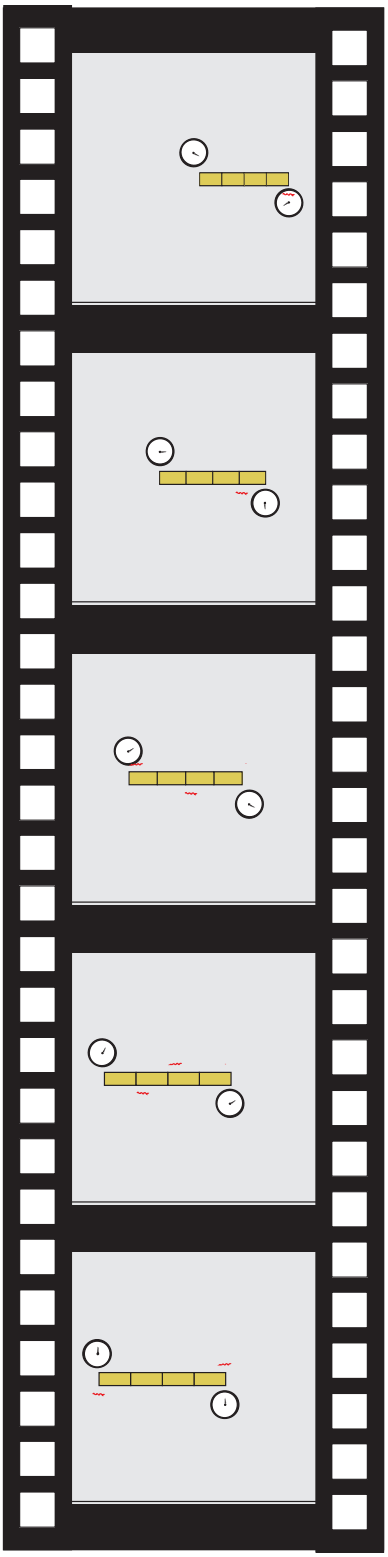

Figure 4. *The traversal of two photons between accelerating clocks.*

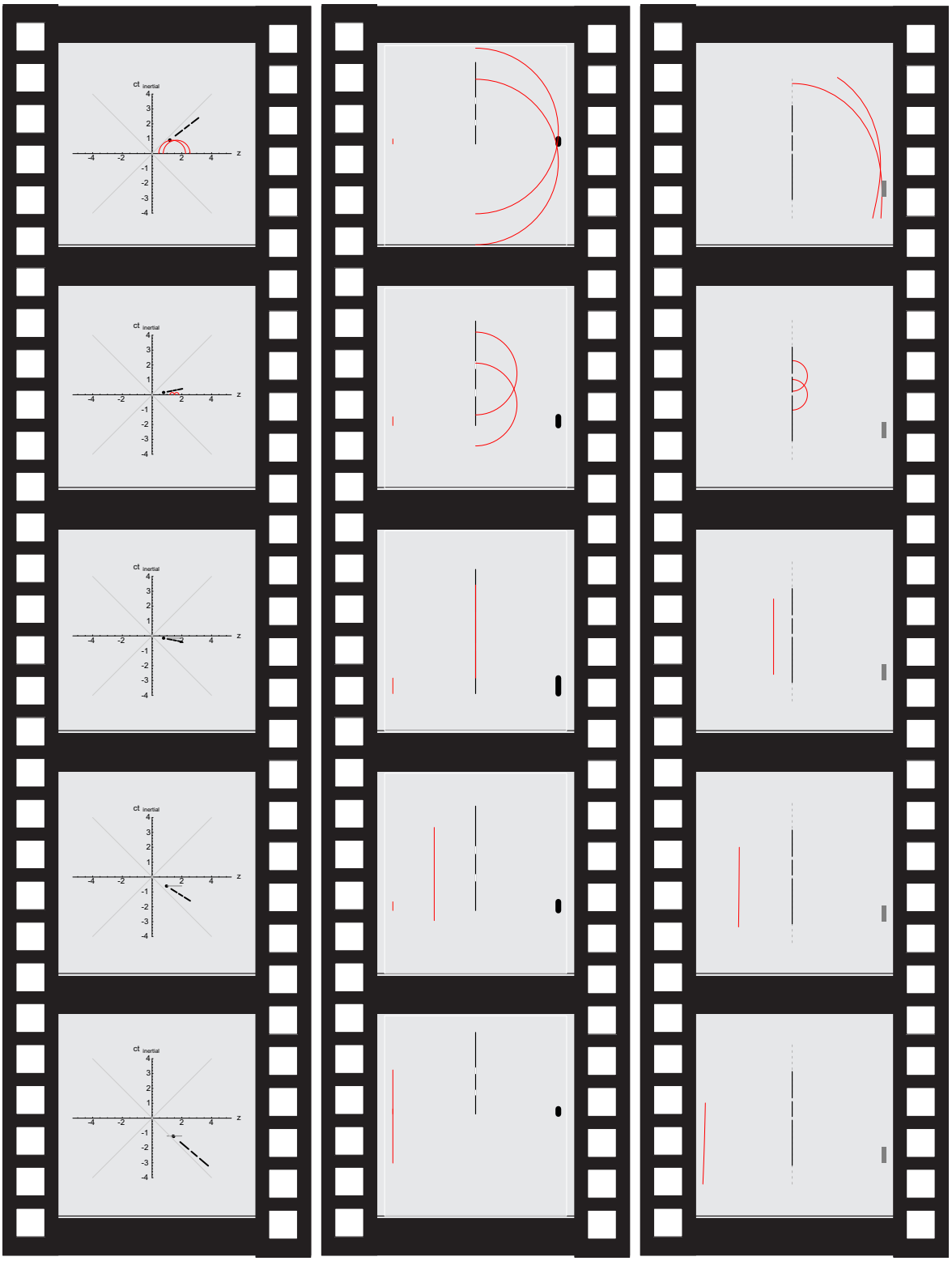

Figure 5. *Various depictions of an inertial wavefront incident upon an accelerating double slit barrier. The frames on the far left depict the wavefront and the accelerating barrier and detector on the Minkowski plane (ct, z) with the x-direction suppressed. In the middle frames, the inertial wavefront, accelerating barrier and accelerating detector are sequentially viewed by a stationary observer. In the frames on the right, the inertial wavefront is viewed relative to the barrier and detector.*

If the relativistic momentum is to take the form $p^j = mu^j = m\frac{dz^j}{d\tau}$, and the relativistic force is of the conservative form $\frac{dp_j}{d\tau} = -\frac{\partial U(z)}{\partial z^j}$, this results in a proper time translation generator of the form

$$K = \frac{p^2}{2m} + U(z) + K_o. \tag{2.10}$$

Description of the dynamics using this canonical proper formulation has the following features:

- K generates translations in the proper time τ of the observed system, with an eigenvalue of the rest energy mc^2.
- The formulation looks very similar to non-relativistic physics, but is fully relativistic! This allows the use of techniques from non-relativistic quantum mechanics for solving relativistic systems.
- It should be noted that this is *not* a Lorentz transformation, rather it is a canonical transformation on the time variable. The temporal coordinate is the proper time of the system, while the momentum and position coordinates (p,x) are those assigned by the observer (which can be highly relativistic). The formulation generates equations of motion of the observers' coordinates for the system in terms of the proper time of that system, not the observers.

The question remains how one determines the constant K_o. This constant can be related to the standard energy E_o measured during production, detection, or a correspondence region of propagation of the quantum state, as will be illustrated in the following examples.

2.4.1. A Plane Wave One of the simplest of quantum systems is that describing a plane wave. A non-interacting quantum system with $U(x) = 0$ can generally have plane wave solutions

$$K = \frac{p^2}{2m} + K_o \quad , \quad K\Psi(x) = mc^2\Psi(x)\,. \tag{2.11}$$

The Hamiltonian formulation for this system has the usual square root form, which connects the constant K_o to the energy of the wave via

$$E_o = \sqrt{(pc)^2 + (mc^2)^2} \quad \Rightarrow \quad K_o = \frac{3(mc^2)^2 - E_o^2}{2mc^2}. \tag{2.12}$$

Thus, the canonical proper energy takes the form

$$\hat{K} = \frac{\hat{p}^2}{2m} + \frac{3(mc^2)^2 - E_o^2}{2mc^2}. \tag{2.13}$$

2.4.2. Canonical proper acceleration Next, consider the uniformly accelerating system examined in section 2.2. Since the solution is already known, one can instead determine the equations of motion.

From (2.5), one can make the identifications

$$\frac{dz}{d\tau} = c\sinh\frac{a\tau}{c} = \frac{\partial K}{\partial p_z}, \text{ and } \frac{dp_z}{d\tau} = \frac{d}{d\tau}\left(m\frac{dz}{d\tau}\right) = ma\cosh\frac{a\tau}{c} = -\frac{\partial K}{\partial z}. \tag{2.14}$$

These equations immediately imply that

$$\frac{\partial K}{\partial p_z} = \frac{p_z}{m}, \text{ and } \frac{\partial K}{\partial z} = -ma\left[\frac{a}{c^2}\left(z - z_{Po}\right)\right], \tag{2.15}$$

which results in a generator for proper time translations of the form

$$K = \frac{p^2}{2m} - ma\left[\frac{a}{2c^2}z^2 + \left(1 - \frac{az_{Po}}{c^2}\right)z\right] + K_o. \tag{2.16}$$

In this equation, z_{Po} is a coordinate of correspondence between the systems.

These steps can be analogously repeated to determine the Hamiltonian formulation for this system:

$$\frac{dz}{dt} = \frac{p_z c}{\sqrt{p_z^2 + (mc)^2}} = \frac{\partial H}{\partial p_z}, \text{ and } \frac{dp_z}{dt} = ma = -\frac{\partial H}{\partial z}. \tag{2.17}$$

This results in a generator for time translations of the form

$$H = \sqrt{(pc)^2 + (mc^2)^2} - maz. \tag{2.18}$$

The last term in (2.18) is akin to the usual mgz form for the gravitational potential energy in elementary physics descriptions of motion in a uniform gravitational field.

To evaluate the integration constant K_o, note that a correspondence can be found such that

$$E_o = \sqrt{(p_{\perp o}c)^2 + (mc^2)^2} - maz_{Po}, \tag{2.19}$$

which results in an integration constant K_o of the form

$$K_o = mc^2 - \frac{(E_o + m\,a\,z_{Po})^2 - (mc^2)^2}{2mc^2} + ma\left[\frac{a}{2c^2}\,z_{Po}^2 + \left(1 - \frac{a\,z_{Po}}{c^2}\right)z_{Po}\right], \tag{2.20}$$

where $z_{Po} = z_o$ is appropriately chosen when $p_z = 0$.

Writing $p^2 = p_x^2 + p_z^2$ in (2.16), one obtains solutions to the equations of motion

$$x(\tau) = x_o + \frac{p_{xo}\tau}{m} \text{ and } z(\tau) = z_{Po} + \frac{c^2}{a}\left(\cosh\frac{a\tau}{c} - 1\right). \tag{2.21}$$

The form of the space-time metric relates the proper time τ to the Minkowski time t via

$$(dc\tau)^2 = (dct)^2 - dx^2 - dz^2 \quad \Rightarrow \quad dct = dc\tau\sqrt{1 + \left(\frac{p_{xo}}{mc}\right)^2 + \sinh^2\frac{a\,\tau}{c}}. \tag{2.22}$$

Thus, the inertial and accelerating time coordinates can be related through the elliptic integral of the second kind:

$$ct = i\,\frac{c^2}{a}\sqrt{1 + \left(\frac{p_{xo}}{mc}\right)^2}E(i\frac{a\tau}{c}|\frac{1}{1 + \left(\frac{p_{xo}}{mc}\right)^2}). \tag{2.23}$$

2.4.3. Semi-classical co-gravitation Consider next a set of freely co-orbiting quantum coherent (neutral) particles that are in composite spherically symmetric states. Experimentally, stationary gravitation itself does not break the coherence of any of the constituent particles. If one assumes that the local energy densities of the co-orbiting coherent quanta serve as gravitational sources generating the background field, then by Birkhoff's theorem (or Gauss' law for gravitational fields as demonstrated by Newton), only the interior (mass) energy density effects the local gravitation at a radial coordinate r. Such spherically symmetric shells can be incoherently combined to construct a co-gravitating system with quantum components.

A semi-classical depiction of this thought experiment analogous to Bohr's analysis of the hydrogen atom is shown in Figure 6. To the extent that any particles are measured interior to

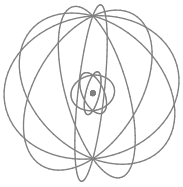

Figure 6. *A semi-classical incoherent sum of nested coherent gravitating particles acting as sources for exterior particles.*

a given co-gravitating particle, those measured particles serve as gravitational sources for any given exterior particle. Assume that the orbital angular momentum of a circularly orbiting mass m must be quantized using Bohr's criterion $L_n = m r_n v_n = n\,\hbar$. The gravitational source mass interior to r_n will be specified by M_n. Using arguments from elementary physics, the speed of the mass and radius parameterizing this orbital must satisfy

$$v_n = \frac{G_N m M_n}{n\hbar} \quad , \quad r_n = \frac{n^2\hbar^2}{G_N m^2 M_n} \quad . \tag{2.24}$$

As long as the dependence M_n assures that the radius increases with quantum number n, one can develop a model where each interior mass contributes as a gravitational source for the subsequent masses. A physical co-gravitating model is constructed by incoherently summing symmetric shells of mass m to give interior mass $M_n = n\,m$ for shell n. Equation (2.24) can then be re-written in terms of the reduced Compton wavelength $\lambda_m \equiv \frac{\hbar}{m\,c}$ of the mass m and the Planck length $L_P \equiv \frac{\hbar}{M_P\,c}$, giving

$$\begin{aligned} a_m = \left(\tfrac{\lambda_m}{L_P}\right)^2 \lambda_m \quad , \quad E_n = -\tfrac{1}{2}\left(\tfrac{L_P}{\lambda_m}\right)^4 m\,c^2 \quad , \\ v_n = \left(\tfrac{L_P}{\lambda_m}\right)^2 c \quad , \quad r_n = n\,a_m \quad , \end{aligned} \tag{2.25}$$

where a_m is a gravitational Bohr radius associated with the mass m, and E_n is the orbital energy of the mass in orbital n. In contrast to the behaviors of electrons in atomic physics, each successive shell of co-gravitating masses experiences increased attraction due to the interior masses. It is interesting to note that the semi-classical speeds of the masses, as well as their gravitational binding energies, are independent of the orbital in this model.

2.4.4. Proper time quantum co-gravitating particles Next, explore the co-gravitation of masses using the canonical proper time formulation. Replacing $U(r) = m\Phi(r)$ as the interaction potential for the mass m in (2.10), the canonical proper time generator K takes the form

$$K = \frac{p^2}{2m} + m\,\Phi(r) + K_o, \tag{2.26}$$

resulting in a canonical equation of motion of the form

$$\frac{d^2x^j}{d\tau^2} = -\nabla_j \Phi(r). \tag{2.27}$$

If this equation of motion is to be consistent with geodesic motion on the geometry

$$\frac{d^2x^j}{d\tau^2} = -\Gamma^j_{\alpha\beta}\frac{dx^\alpha}{d\tau}\frac{dx^\beta}{d\tau}, \tag{2.28}$$

then for a stationary distribution with $\frac{dx^j}{d\tau} = 0$ geodesic motion requires that

$$\frac{d^2x^j}{d\tau^2} = \frac{1}{2}g^{j\mu}\frac{\partial g_{00}}{\partial x^\mu}\left(\frac{dx^0}{d\tau}\right)^2. \tag{2.29}$$

As a quick calculation, consider a generalization of the exterior Schwarzschild geometry obtained by simply giving the mass a radial dependency:

$$ds^2 = -\left(1 - \frac{2G_N M(r)}{c^2 r}\right)(dct)^2 + 2\sqrt{\frac{2G_N M(r)}{c^2 r}}\,dct\,dr + dr^2 + r^2\left(d\vartheta^2 + \sin^2\vartheta\,d\varphi^2\right). \tag{2.30}$$

If there is no radial dependency in the mass $M(r)$, then this form can be diagonalized into the Schwarzschild form using the Schwarzschild time $t_S \neq t$. However, (2.30) has no physical singularities except perhaps at the origin $r = 0$ for a radially dynamic geometry. For this metric form, the potential that satisfies (2.29) and (2.27) has the form

$$\Phi(r) = -\frac{G_N M(r)}{r}, \tag{2.31}$$

which is the same as that for Newtonian gravitation, but includes space-time curvatures! Substitution of this metric into Einstein's equation gives

$$G^0{}_0 = \frac{1}{r^2}\frac{\partial}{\partial r}\frac{2G_N M(r)}{c^2} \quad \Rightarrow \quad M(r)c^2 = \int_0^r T^0{}_0(r')\,4\pi r'^2 dr', \tag{2.32}$$

which is precisely the interior mass corresponding to the energy density that curves the space-time.

A general quantum co-gravitating system is developed by considering a stationary mass m gravitating due both to a source mass M_ℓ which depends only on ℓ (the angular momentum quantum number associated with the stationary quantum state), as well as self gravitation. The proper energy form satisfies the stationary equation given by

$$\begin{gathered}\left(\tfrac{\hat{p}^2}{2m} - \tfrac{G_N m M_\ell(r)}{r} + K_\ell\right)\psi_{\ell\ell_z}(r,\theta,\phi) = mc^2\;\psi_{\ell\ell_z}(r,\theta,\phi) \quad , \\ \psi_{\ell\ell_z}(r,\theta,\phi) = R_\ell(r)Y_\ell^{\ell_z}(\theta,\phi).\end{gathered} \tag{2.33}$$

Re-writing the momentum squared operator as $\mathbf{p}\cdot\mathbf{p} = -\hbar^2\left[\frac{1}{r^2}\frac{\partial}{\partial r}\left(r^2\frac{\partial}{\partial r}\right) - \frac{\mathbf{L}\cdot\mathbf{L}}{\hbar^2 r^2}\right]$, one notes that spherically symmetric forms are constructed by summing over the $2\ell+1$ values of the index ℓ_z using the spherical harmonic addition theorem,

$$\sum_{\ell_z=-\ell}^{\ell}\left|Y_\ell^{\ell_z}(\theta,\phi)\right|^2 = \frac{2\ell+1}{4\pi}\;P_\ell(1).$$

The reduced radial wavefunctions defined by $u_\ell(r/a_m) \equiv rR_\ell(r)$ can be parameterized in terms of the dimensionless variable $\zeta \equiv r/a_m$, where as before $a_m \equiv \frac{\hbar^2}{G_N m^3}$. This allows the equation (2.33) to be re-written in a dimensionless form:

$$\frac{d^2u_\ell(\zeta)}{d\zeta^2} - \frac{\ell(\ell+1)}{\zeta^2}\,u_\ell(\zeta) + \left(\frac{2}{\zeta}\right)\left(\frac{M_\ell(\zeta)}{m}\right)u_\ell(\zeta) = \epsilon_\ell\,u_\ell(\zeta)\;, \tag{2.34}$$

where the dimensionless expression $\epsilon_\ell = -2\left(\frac{\lambda_m}{L_P}\right)^4 \frac{mc^2 - K_\ell}{m\,c^2}$ parameterizes the gravitational binding energy of the mass m.

In analogy to the semi-classical case previously presented, the interior mass will be presumed to be composed of particles of mass m_ℓ:

$$M_\ell(\zeta) = \int_0^\zeta \rho_{mass}(\zeta')\, d\zeta' = \int_0^\zeta \sum_{\text{all } \ell'} n_{\ell'}\, m_{\ell'}\, u_{\ell'}^2(\zeta')\, d\zeta', \tag{2.35}$$

which represents an incoherent sum of the co-gravitating interior masses $m_{\ell'}$. This means that in (2.34), the particle masses appear only in ratios, an explicit demonstration of the elegance of the principle of equivalence.

For illustrative purposes, consider a single s-wave particle of mass m self-gravitating in a spherically symmetric manner. The gravitating distribution takes the form demonstrated in Figure 7. The metric component from (2.30) which has the form $g_{00} = -\left(1 - \frac{2G_N M(r)}{c^2 r}\right)$, can

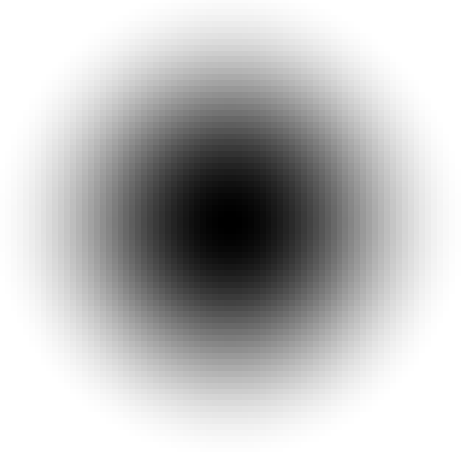

Figure 7. *Probability density of a single self gravitating proper coherent mass.*

be expressed in terms of the dimensionless functions

$$\frac{2G_N M(r)}{c^2 r} = 2\left(\frac{m}{M_P}\right)^4 \frac{\mathcal{P}_{interior}(\zeta)}{\zeta}, \tag{2.36}$$

where $\mathcal{P}_{interior}(\zeta)$ represents the integrated probability density interior to radial coordinate $\zeta = r/a_m$. Notice that in this expression, the particle mass appears only in terms of its ratio relative to the Planck mass M_P, with $\mathcal{P}_{interior}(\zeta)$ defining a *general* functional form in the coordinate ζ.

2.5. Global causal structure of gravitating mass

Quite often, diagrammatic techniques are useful for visualizing and interpreting important aspects of a physical model. Penrose diagrams are space-time diagrams that have the following properties:

- Light rays travel along straight lines with slope ± 1
- The whole of space-time fits on a single page

These properties allow the diagrams to be used to determine the global causal structure of the given geometry.

Consider for example the Penrose diagram Figure 8 for flat Minkowski space-time. On the

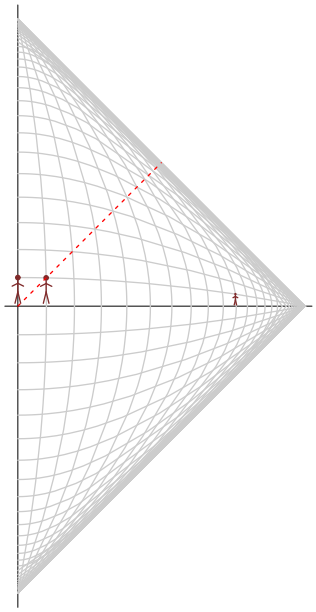

Figure 8. *Global causal structure of Minkowski space-time. The vertical axis represents ct (i.e., $r = 0$), and the horizontal axis represents r (i.e., $ct = 0$). The left boundary represents an observer at rest at $r = 0$. The lower right boundary (often referred to as* skri minus*, or past light-like infinity) represents an outgoing light ray emitted from $r = 0$ at $t = -\infty$, reaching $r = \infty$ at $t = 0$. The upper right boundary (often referred to as* skri plus*, or future light-like infinity) represents an ingoing light ray emitted from $r = \infty$ at $t = 0$, reaching $r = 0$ at $t = +\infty$. Each point on the diagram represents a spherical surface (i.e., all ϑ, φ) at a given time.*

diagram, observers of the same proper height are represented at $r = 0$, $r = 1$, and $r = 10$. The scale is seen to compress in distant locations and times in order to contain the whole of space-time on a finite diagram. An outgoing light-beam emitted from $r = 0$ at $t = 0$ traverses equal spatial and temporal displacements on the diagram as displayed as a dashed line of slope 1. No event above this light-like line can be a cause of an event below it. However, there is no spatial region in Minkowski space-time that is causally inaccessible from another over all times.

Energy density will curve the local space-time geometry, and modify the Penrose diagram, sometimes to the extent that it will change the global causal structure of the geometry (as with a black hole). For a dense star or self-gravitating mass such as in Figure 7, light rays are blue shifted when approaching the center $r = 0$, and red shifted when receding. Using the conformal space-time coordinates (i.e., coordinates that preserve the slope of light-like trajectories) needed to construct a Penrose diagram, a ingoing light beam from past light-like infinity that reflects off of (or passes through) $r = 0$ traverses a modified geometry, as illustrated in Figure 9. The curvature effect at the time-like center $r = 0$ is due to the high energy density, plotted as a proportionate density of shading on the diagram. For a high enough energy density, the curvature near the center is eventually large enough to form a black object (which has a trapping region within which outgoing light rays have decreasing radial coordinate) or a black hole (which

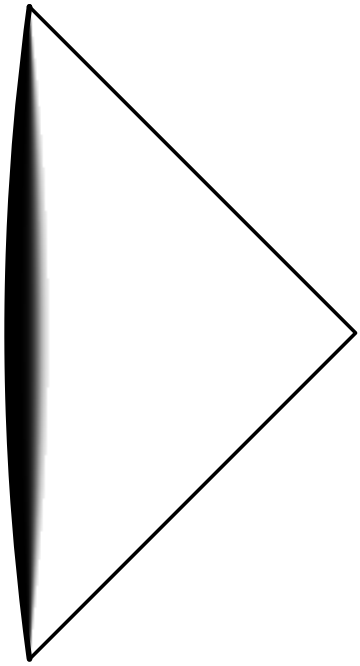

Figure 9. *Penrose diagram for a self gravitating high energy density. The global causal structure is the same as that of Minkowski space-time.*

manifests a *horizon*, within which there can be no cause that affects the exterior). In Figure 9, the Schwarzschild (vacuum) geometry is valid in the region exterior to any energy density. The past and future light-like infinities are familiar from the Minkowski space-time behavior of the geometry far away from its center.

3. A Non-Singular Black Hole

One notable feature of (2.36) is that the term calculated from the general equation of motion depends only upon the dimensionless radial variable $\zeta = r/a_m$, resulting in solutions for self gravitating masses that are always of the functional form demonstrated in Figure 7, regardless of the size of the mass m. This means that only the term involving the ratio $\left(\frac{m}{M_P}\right)^4$ determines when this distribution can result in a sign change in a metric component at some finite radial coordinate ζ. For the self-gravitating solution presented, no black hole is generated unless $g_{00} > 0$ which occurs only when $m \gtrsim 0.63 M_P$. Significantly for this calculation, *quantum non-locality prevents a singularity from ever forming regardless how large the self-gravitating mass!*

As a concrete example, consider a non-singular Planck mass black hole $m = M_P$. The metric component $-g_{00}(\zeta)$ is plotted in Figure 10. For large ζ far from the black hole, the metric takes the Minkowski form $g_{00} \to -1$. Similarly, very near the center $\zeta \to 0$ the metric likewise takes a Minkowski form. At the center, the metric and all curvatures are finite because of the quantum distribution consistent with non-locality and the uncertainty principle. However, in the region between $0.4 \lesssim \zeta \lesssim 2$, the component g_{00} is positive, defining a trapping region within which outgoing light rays will have decreasing radial coordinate ζ. Thus, the global geometry separates into three regions: an exterior region, a trapping region, and an interior region, as illustrated in the Penrose diagram for this system in Figure 11. On the diagram, the exterior region is labeled on the lower right hand part of the diagram, and the interior region is the

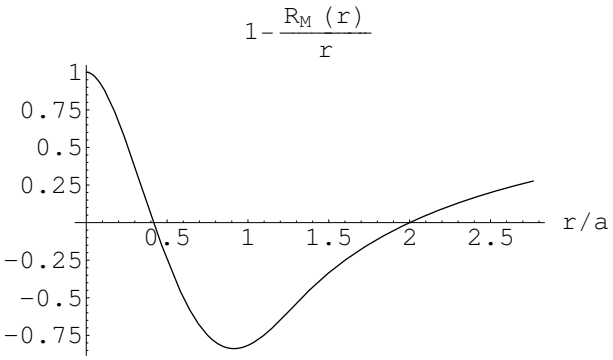

Figure 10. *Plot of the time-time component of the space-time metric for a self-gravitating Planck sized mass as a function of the dimensionless radial coordinate* $\zeta = \frac{r}{a_{M_P}} = \frac{r}{L_P}$.

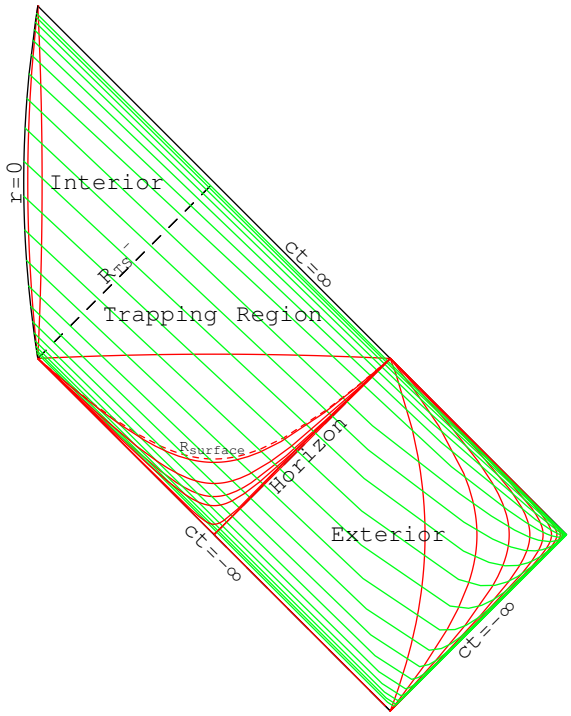

Figure 11. *Penrose diagram of a non-singular Planck mass black hole.*

upper left hand part of the diagram. The horizon of the black hole separates the exterior region from the trapping region, and the inner trapping surface R_{TS} separates the interior region from the trapping region. Curves of constant time are everywhere space-like volumes, all terminating on $r = 0$ (which is time-like and non-singular) and at the right apex of the diagram $r = \infty$ as shown. Curves of constant radial coordinate are vertical in the interior and exterior regions, but horizontal in the trapping region, as illustrated. Thus all light-like and time-like trajectories necessarily have decreasing radial coordinate in the trapping region. There are no exotic energy densities in the interior and exterior regions.

In the Penrose diagram 11, ingoing time-like or light-like trajectories can connect external causes to effects in the trapping region or interior. However, all time-like or light-like trajectories in the interior always terminate on a future boundary of the interior. This defines the object as a black hole.

3.1. General Stationary Spherically Symmetric Distributions

The Schwarzschild geometry only represents the vacuum solution of a stationary, spherically symmetric system exterior to any non-vanishing energy density. The most general, stationary, radially symmetric metric form that is also valid in the interior region with non-vanishing energy density can be written in the form[3]

$$ds^2 = -\left(1+\frac{2[V(r)+V_o(r)]}{c^2}\right)(dct)^2 + 2\sqrt{\left(-\frac{2V(r)}{c^2}\right)\frac{\left(1+\frac{2[V(r)+V_o(r)]}{c^2}\right)}{\left(1+\frac{2V(r)}{c^2}\right)}}\,dct\,dr + dr^2 + r^2\left(d\vartheta^2+\sin^2\vartheta\,d\varphi^2\right), \tag{3.1}$$

which reduces to the form (2.30) in the exterior region $V_o \to 0$ and $V(r) \to -\frac{G_N M}{r}$.

The canonical proper time generator for the metric (3.1) consistent with previous assumptions takes the form

$$K = \frac{p^2}{2m} + m\,\Phi(r) + K_o \Rightarrow \frac{\partial}{\partial r}\Phi(r) = \frac{1+\frac{2V(r)}{c^2}}{1+\frac{2[V(r)+V_o(r)]}{c^2}}\frac{\partial}{\partial r}[V+V_o] \tag{3.2}$$

In the interior region, the solution for the canonical potential $\Phi(r)$ is not trivially related to general forms of the functions $V(r)$ and $V_o(r)$ as it was for the metric (2.30), but should be calculable in terms of an integral. In addition, the condition of isotropy in Einsteins equation, as well as any equation of state, relates V_o to V, which is again determined via the quantum distribution of a self-gravitating mass. This means that the calculation of a physically meaningful non-singular self-gravitating systems should be straightforward, though complicated. It is expected that even a black hole resulting from such a non-singular self-gravitating system should have no exotic energy density (i.e., no space-like energies, thereby violating energy conditions) anywhere on the geometry.

Substitution of the metric (3.1) into Einstein's equation directly relates the geometry to the energy-momentum densities consistent with that geometry. By direct calculation, the $T^0{}_0$ component of the energy-momentum tensor takes the form

$$T^0{}_0 = \frac{1}{r^2}\frac{\partial}{\partial r}\left(\frac{rV(r)c^2}{4\pi G_N}\right) \tag{3.3}$$

This implies that if the function $V(r)$ is rewritten in the general form $V(r) = -\frac{G_N M(r)}{r}$, then

$$M(r)c^2 = -\int_0^r T^0{}_0\,4\pi\tilde{r}^2 d\tilde{r}. \tag{3.4}$$

One can immediately interpret the function $M(r)$ as the mass interior to a spherical region of radius r.

4. Beyond the Canonical Proper Generator K: Scattering in Quantum Gravity

To end the discussion, a generalization of the canonical proper formulation beyond the eigenvalue problems discussed so far will be examined. Consider an invariant form for the generator K expressed as follows:

$$\hat{K}|\psi_m\rangle = i\hbar\frac{dx^\mu}{d\tau}\frac{\partial}{\partial x^\mu}|\psi_m\rangle = -u^\mu\hat{P}_\mu|\psi_m\rangle = mc^2|\psi_m\rangle. \tag{4.5}$$

Dynamics expressed in this form typically represent substantive quantum flows[12]. As previously discussed, although the canonical variables used to develop expressions for the generator K are generally those of observers in arbitrary motions, its eigenvalue is the invariant energy of the system.

An analogous expression is given by the Dirac equation[14] for spinor fields. Consider the expression on a locally flat space given by

$$\frac{1}{\Gamma}\mathbf{\Gamma}^\mu\hat{P}_\mu\mathbf{\Psi}^{(\Gamma)}_{(\gamma)}(m\vec{u},J,s_z) \;=\; -\frac{(\gamma)}{\Gamma}mc\,\mathbf{\Psi}^{(\Gamma)}_{(\gamma)}(m\vec{u},J,s_z), \tag{4.6}$$

where $\frac{(\gamma)}{\Gamma} = \pm 1$ for the $\Gamma = \frac{1}{2}$ representation. The substantive flow field for general coordinates can be expressed in terms of the curvilinear matrix-valued 4-velocity $\mathbf{U}^\beta$ defined using the principle of equivalence

$$\mathbf{U}^\beta(x) \equiv \frac{\partial x^\beta}{\partial\xi^\mu}\frac{\mathbf{\Gamma}^\mu}{\Gamma}. \tag{4.7}$$

In this expression, the ξ^μ are locally flat coordinates that can always be found. An algebra that consistently develops this dynamics is demonstrated in the next section.

4.0.1. Extended Lorentz Group Commutation Relations

The commutation relations of the Lorentz group algebra can be extended in a manner consistent with the Dirac matrices[15, 16] as follows:

$$\begin{gathered}
[J_j\,,\,J_k] \;=\; i\hbar\,\epsilon_{jkm}\,J_m, \quad [J_j\,,\,K_k] \;=\; i\hbar\,\epsilon_{jkm}\,K_m, \quad [K_j\,,\,K_k] \;=\; -i\hbar\,\epsilon_{jkm}\,J_m, \\
\left[\Gamma^0\,,\,\Gamma^k\right] \;=\; \tfrac{i}{\hbar}\,K_k, \qquad [\Gamma^0\,,\,J_k] \;=\; 0, \qquad [\Gamma^0\,,\,K_k] \;=\; -i\hbar\,\Gamma^k, \\
\left[\Gamma^j\,,\,\Gamma^k\right] \;=\; -\tfrac{i}{\hbar}\,\epsilon_{jkm}\,J_m, \quad [\Gamma^j\,,\,J_k] \;=\; i\hbar\,\epsilon_{jkm}\,\Gamma^m, \quad [\Gamma^j\,,\,K_k] \;=\; -i\hbar\,\delta_{jk}\,\Gamma^0.
\end{gathered} \tag{4.8}$$

The operators Γ^β are chosen to be dimensionless, while the angular momentum J_k and boost K_j generators have dimensions of $\hbar$. Representations are labeled by the parameter Γ, which must take on integer or half-integer values. Microscopic causality[3] then requires that the associated spinor fields must satisfy boson statistics for integer values and fermi statistics for half-integer values of Γ.

4.0.2. A closed set of extended Poincare operators The introduction of operator valued group generators $\hat{\Gamma}^\beta$ that extend the Lorentz group algebra require the introduction of an additional scalar operator $\hat{\mathcal{M}}_T$ when space-time translations are included, in order to close the resulting extended group algebra[3]. Any closed group of operations must satisfy the algebraic Jacobi identities, $[A,[B,C]]+[C,[A,B]]+[B,[C,A]]=0$. The non-vanishing commutators involving the operators $\hat{P}_\mu$ and $\hat{\mathcal{M}}_T$ that satisfy the Jacobi identities[17] and insure group closure are given by

$$\begin{gathered}
[J_j\,,\,P_k] \;=\; i\hbar\,\epsilon_{jkm}\,P_m, \quad [K_j\,,\,P_0] \;=\; -i\hbar\,P_j, \quad [K_j\,,\,P_k] \;=\; -i\hbar\,\delta_{jk}\,P_0, \\
[\Gamma^\mu\,,\,P_\nu] \;=\; i\,\delta^\mu_\nu\,\mathcal{M}_T c, \quad [\Gamma^\mu\,,\,\mathcal{M}_T] \;=\; \tfrac{i}{c}\,\eta^{\mu\nu}\,P_\nu.
\end{gathered} \tag{4.9}$$

An extended Poincare group Casimir operator is constructed using the Lorentz invariants

$$\mathcal{C}_m \equiv \mathcal{M}_T^2 c^2 - \eta^{\beta\nu} P_\beta P_\nu. \tag{4.10}$$

The label m in the Casimir $\mathcal{C}_m$ is a mass that parameterizes the eigenstates used to construct finite dimensional representations. Due to the form of the group Casimir, eigenvalues of the hermitian operator $\mathcal{M}_T$ will be referred to as the *transverse mass* of the state.

The transverse mass operator $\mathcal{M}_T$ introduced to close the algebra can be shown to have non-vanishing values only for massless particles $\eta^{\beta\nu} P_\beta P_\nu = 0$. For massless particles, $\mathcal{M}_T$ serves as the generator for affine translations along their light-like trajectories . Non-vanishing eigenvalues for $\mathcal{M}_T$ provide a mechanism for dynamic mixing of massless particles of differing transverse mass.

This formulation has direct applicability in relativistic cluster decomposable and unitary multi-particle scattering theory consistent with correspondence to classical, non-relativistic dynamics. However, the approach here utilized differs from that in reference [18], wherein space-time curvature is introduced via the generalization $\{\gamma^\mu, \gamma^\nu\} = -\eta^{\mu\nu}\mathbf{1} \rightarrow -g^{\mu\nu}(x)\,\mathbf{1}$ for the Dirac matrices γ^μ[19]. In general, $\{\mathbf{\Gamma}^\mu, \mathbf{\Gamma}^\nu\} \neq -\eta^{\mu\nu}\mathbf{1}$ (except for the $\Gamma = \frac{1}{2}$ representation which reproduces the Dirac equation). Rather, the approach presented here introduces space-time curvature directly through the principle of equivalence, along with the introduction of the Minkowski metric through the commutation relations between the operators $\hat{\Gamma}^\mu$, along with Lorentz invariance of the product $\hat{\Gamma}^\mu \hat{P}_\mu$.

5. Discussion and Conclusions

The physical universe is inherently quantum mechanical at its most fundamental level. Although quantum physics is non-deterministic, classical behaviors emerge when measurements cluster very near to quantum averaged values, providing validity to deterministic classical models.

Experiments demonstrate that the known gravitational effects cannot break the quantum coherence of gravitating systems in order to establish the needed space-time dependent phase relationships. In particular, gravitating quantum systems establish interference across regions of space-time described using classical ideas of geometric relationships. This means that the use of classical space-time relationships is sufficient to describe all known data, even for gravitating quantum coherent systems. Therefore, the approach taken here is to use expectation values of the energy-momentum tensor in Einstein's equation to generate the consistent curvatures of classical geometries upon which measurements take place. Covariance must connect such geometries to any other approach (e.g. using quantized coordinates, etc.) through appropriate correspondence, as long as Einstein's equation remains consistent with experiment.

Locally inertial coordinates can always be found for freely gravitating systems. Generally, one expects that the particle mass of a freely falling system is a parameter best described using the proper reference frame dynamics of that system. The proper time of a particle of defined mass provides a very convenient parameter for describing that dynamics, since it is the temporal variable of most relevance to the particle itself. This has been the primary motivation for the formulation of canonical proper gravitation as developed in this paper.

Since canonical proper gravitation embraces equivalence, it formulates quantum gravity in a way that is consistent with the formulation of classical gravitation by Einstein. It preserves quantum linearity, unitarity and classical correspondence. Expectation values of quantum energy densities generate space-time curvatures consistent with general relativity. Furthermore, it has been demonstrated that the formation of a singularity during gravitational collapse is not inevitable, due to quantum non-locality (i.e., the non-commutivity of position and momentum, resulting in the uncertainty principle). Since quantum non-locality is expected to continue to be a fundamental characteristic of known physical energies, exotic geometric objects (e.g. black holes, etc.) need not necessarily imply exotic or singular energy densities, in principle.

Acknowledgments
The author wishes to acknowledge the International Association for Relativistic Dynamics for its continuing support of novel approaches towards understanding outstanding problems in theoretical physics. In addition, the author appreciates the efforts of Tepper Gill in developing the canonical proper time formulation of relativistic systems.

References
[1] Einstein A, Podolsky B, and Rosen N 1935 *Phys. Rev.* **47**, 777
[2] Bell J S 1964 *Physics* **1**, 195
[3] Lindesay J 2013 *Foundations of Quantum Gravity* (Cambridge: Cambridge University Press)
[4] Colella R, Overhauser A W, and Werner S A 1975 Observation of Gravitationally Induced Quantum Interference *PRL* **34** 1472-4
[5] Muller H, Peters A, and Chu S 2010 A precision measurement of the gravitational redshift by the interference of matter waves *Nature* **463** 926-9
[6] Levi B G 2004 Ultracold gases of fermionic atoms offer another path to atom interferometry *Physics Today* August 25
[7] Roati G, de Mirandes E, Ferlaino F, Ott H, Modugno G, and Inguscio M 2004 *Phys. Rev. Lett.* **92**, 230402
[8] Will C M 2006 The Confrontation between General Relativity and Experiment *Preprint* arXiv:gr-qc/0510072v2
[9] Susskind L and Lindesay J 2005 *An Introduction to Black Holes, Information, and the String Theory Revolution: The Holographic Universe* (Singapore: World Scientific)
[10] Lindesay J and Gill T 2004 Canonical Proper Time Formulation for Physical Systems *Foundations of Physics* **34**(1), 169-82
[11] Gill T and Lindesay J 1993 Canonical Proper Time Formulation of Relativistic Particle Dynamics *International Journal of Theoretical Physics* **32**, 2087-98
[12] Lindesay J V and Morrison H L 1985 The Geometry of Quantum Flow *Mathematical Analysis of Physical Systems*, ed R E Mickens, (NewYork: Van Nostrand Reinhold) p 135
[13] Dirac P A M 1928 *Proc. Roy. Soc.* (London) **A117** 610
[14] Dirac P A M 1928 *Proc. Roy. Soc.* (London) **A118** 351
[15] Lindesay J 2003 Linear Spinor Field Equations for Arbitrary Spins *Preprint* arXiv:math-ph/0308003
[16] Lindesay J 2003 Group Structure of an Extended Lorentz Group *Preprint* arXiv:math-ph/0309060
[17] Lindesay J 2003 An Extended Poincare Algebra for Linear Spinor Field Equations *Preprint* arXiv:math-ph/0308015
[18] Brill D and Wheeler J 1957 Interaction of Neutrinos and Gravitational Fields *Rev. Mod. Phys.* **29** 465
[19] Bade W L and Jehle H 1953 An Introduction to Spinors *Rev. Mod. Phys.* **25**, 714